

Article

Fully Relativistic Electron Impact Excitation Cross-Section and Polarization for Tungsten Ions

Priti, Dipti, Lalita Sharma and Rajesh Srivastava *

Department of Physics, Indian Institute of Technology Roorkee, Roorkee 247667, India;
E-Mails: prtidph@iitr.ac.in (P.); diptidph@iitr.ac.in (D.); lalitfph@iitr.ac.in (L.S.)

* Author to whom correspondence should be addressed; E-Mail: rajsrfph@iitr.ac.in;
Tel.: +91-1332-285-754; Fax: +91-1332-273-560.

Academic Editor: Bastiaan J. Braams

Received: 16 February 2015 / Accepted: 10 April 2015 / Published: 28 April 2015

Abstract: Electron impact excitation of highly charged tungsten ions in the framework of a fully relativistic distorted wave approach is considered in this paper. Calculations of electron impact excitation cross-sections for the M- and L-shell transitions in the tungsten ions W^{n+} ($n = 44–66$) and polarization of the decay of photons from the excited tungsten ions are briefly reviewed and discussed. New calculations in the wide range of incident electron energies are presented for M-shell transitions in the K-like through Ne-like tungsten ions.

Keywords: Electron-impact excitation; highly charged tungsten ions; relativistic distorted wave; polarization

1. Introduction

Special physical properties of tungsten such as its highest melting point and lowest metal pressure amongst metals make it a potential candidate in fusion engineering where tungsten can be used as a potential plasma facing material. Various charge species of tungsten are predicted to be present in the high-temperature and low-density divertor plasma of the International Thermonuclear Experiment Reactor (ITER) tokamak [1–3]. Tungsten ions, which move into a tokamak will not be completely ionized even in the hot core, thus causing strong X-ray emission over a wide range of temperatures. Since electron induced processes are anticipated to be among the dominant ones, it is likelihood that tungsten ions will get excited by collision with plasma electrons and will decay by emitting radiation.

Thus information on the electron impact excitation cross-sections as well as the polarization of the radiation emitted due to decay of the excited state will facilitate a thorough understanding of the spectra for plasma diagnostics. For example, the ion temperature of the ITER core plasma can be assessed with the help of such diagnostics. Polarization studies play an important role in understanding the plasma properties, as X-ray polarization spectroscopy is a useful diagnostic tool for measuring the velocity distribution of hot electrons propagating in plasma created with a high intensity laser pulse [4]. It has also been employed to measure the energy component associated with the cyclotron motion of the beam electrons in the Livermore electron beam ion trap (EBIT) [5].

The understanding and modeling of such a plasma rely on the knowledge of accurate atomic data for ion species encountered in the plasma [6]. The International Atomic Energy Agency (IAEA) has constituted a committee consisting of leading scientists from all over the world in order to encourage the production and exchange of a variety of tungsten data required to facilitate the growth of ITER and other fusion applications. One of the authors, R.S. has been a member of this committee. The initiative taken by IAEA has led to extensive experimental and theoretical investigations related to emission spectra, energy levels, transition rates, ionization, excitation, radiative recombination and dielectronic recombination *etc.*, of highly charged tungsten ions [7]. As a coordinated effort to cater the need of atomic data of various ionic stages of tungsten, thereby assisting in the design and development of ITER, we have undertaken the present project to provide reliable cross-section data for excitation of ions by electron impact.

X-ray spectroscopy utilizing emissions from L-shell as well as M-shell tungsten ions is an attractive option for tokamak plasma diagnostics [8–22]. The temperature of the ITER core will be sufficiently high to produce the L-shell tungsten ionic charged states. Emissions from the L-shell ionic charged states are proposed to be the main diagnostics of the ITER plasma using a core imaging X-ray spectrometer (CIXS) [23]. There has also been interest in the study of emissions from M-shell charged states of tungsten, which will be present in considerable amount in the ITER core under ohmic plasma operations. In this context, we have performed fully relativistic distorted wave (RDW) calculations to obtain cross-sections for various M- and L-shell transitions due to electron impact excitation of highly charged tungsten ions W^{n+} where n varies from 44 to 66. This work is undertaken in the light of recent measurements in an electron beam ion trap at the Lawrence Livermore National Laboratory reported by Beiersdorfer and his co-workers [19–22] in which they identified a number of intense lines in the L- and M-shell spectra of various tungsten ions. The electron excitation processes corresponding to these lines are studied in detail due to the importance of the cross-section data to identify and interpret the spectroscopic data of the tungsten ions. Also anticipating the importance of information about the polarization [24] of the subsequent emission arising from electron impact anisotropically excited states of tungsten ions, results are obtained for polarization of the photon emissions utilizing the calculated magnetic sublevel excitation cross-sections. It should be noted here that in the present work we have considered only the electron impact inner L- and M-shell excitations to specifically selected excited states which lead to X-ray emissions on its decay back to the initial state [25–27]. No attempt has been made to take into account the population of such selected excited states from other lower lying excited states or from the radiative decay of the upper lying excited states. These later effects along with other excitations and various possible processes can be incorporated when one does the complete plasma modeling separately through a suitable collisional radiative model [28]. It is worth mentioning here that there are no reports on the

direct experimental measurements of electron impact excitation cross-sections for these tungsten ions and thus, theoretical predictions are of prime importance.

The article is organized as follows. In Section 2 we give necessary details of the theoretical method employed while in Section 3 we provide the review of our calculations performed for L- and M-shell electron excitation of tungsten ions [25–27]. Further, new results are obtained for M-shell excitation in K-like through Ne-like tungsten ions, which are reported and discussed in Section 4.

2. Theoretical Background

We employed the RDW theory [29] to study the electron impact excitation of various charge species of tungsten ions. The general transition matrix for the excitation of an ion from initial state $|\alpha_a J_a M_a\rangle$ to final state $|\alpha_b J_b M_b\rangle$ can be written as

$$T_{a \rightarrow b}^{DW} = \langle \alpha_b J_b M_b \mu_b | V - U_b | \alpha_a J_a M_a \mu_a \rangle \tag{1}$$

Here J and M denote the total angular momentum and its z-component of the atomic state and μ refers to the spin projection of the free electron while α represents all other quantum numbers necessary to specify the ion's state. V is the projectile electron and target ion interaction potential given by

$$V = -\frac{Z - N}{r_{N+1}} + \sum_{i=1}^N \frac{1}{|\mathbf{r}_i - \mathbf{r}_{N+1}|} \tag{2}$$

Here \mathbf{r}_i ($i = 1, \dots, N$) and \mathbf{r}_{N+1} denote, respectively, the position coordinates of the ionic N electrons and projectile electron with respect to the nucleus of the ion. The distortion potential U_b is chosen to be the spherically averaged static potential V_{static} of the excited state of the ion and it can be obtained using the following expression,

$$V_{static}(r_{N+1}) = -\frac{Z - N}{r_{N+1}} + \sum_{\substack{j \in \text{all} \\ \text{subshells}}} \omega_j \int_0^\infty [P_{n_j \kappa_j}^2(r) + Q_{n_j \kappa_j}^2(r)] \frac{1}{r} dr \tag{3}$$

where P and Q represent the larger and smaller components of the radial part of the target ion wavefunction, ω_j is the occupation number of the j th subshell and the electron in it is represented by quantum numbers $n_j \kappa_j$. This choice of distortion potential leads to the most congruous results in the distorted-wave approximation [30,31].

With our normalization of the distorted waves, the magnetic sublevel cross-section for the excitation of the ion from a fine-structure initial level with angular momentum J_a to a higher lying level J_b is given by

$$\sigma(\alpha_b J_b M_b) = \sigma_{M_b} = (2\pi)^4 \frac{k_b}{2(2J_a + 1)k_a} \sum_{M_a \mu_a \mu_b} \int \langle \alpha_b J_b M_b \mu_b | V - U_b | \alpha_a J_a M_a \mu_a \rangle^2 d\Omega \tag{4}$$

Here the integral has been carried over the scattering angles of the scattered electron. k_a and k_b are the momenta of the projectile and scattered electrons, respectively. The total cross-section $\sigma(\alpha_b J_b)$ can be obtained by summing over electron-impact excitation cross-sections $\sigma(\alpha_b J_b M_b)$ for all magnetic sub-states of final state of the ion *i.e.*, $\sigma(\alpha_b J_b) = \sum_{M_b} \sigma(\alpha_b J_b M_b)$. All these calculations are performed in

Collision frame of reference which is a standard choice for numerical calculations, where the

quantization axis (z -axis) is parallel to the incident electron beam direction while the y -axis is perpendicular to the scattering (xz) plane which consists of the direction of incident as well as scattered electron.

The reliability of the cross-sections depends on the accuracy of the target wavefunctions used in the calculation. The wavefunctions are obtained within Dirac-Fock approximation by using GRASP92 [32]/GRASP2k code [33]. The quality assessment of the bound state wavefunctions of the target ion is done by comparing our calculated oscillator strength and the excitation energy of the transition in question with the corresponding values available from measurements and other reliable theoretical methods. These bound state wavefunctions are not only used to describe the target ions in the initial and final states but are also used to calculate the distortion potential. Using these, the projectile electron distorted wavefunctions are obtained by solving the coupled Dirac equations with appropriate boundary conditions. Thereafter, a transition matrix (Equation (1)) is calculated and finally cross-sections are obtained by using Equation (4).

Using the density matrix theory, one can explore the magnetic sub-level excitation cross-sections $\sigma(\alpha_b J_b M_b)$ further to obtain the polarization of the emitted photon due to decay of the electron impact excited $|\alpha_b J_b\rangle$ state of ions to any lower state $|\alpha_0 J_0\rangle$. In general, the photons are detected in the y -direction perpendicular to the scattering xz -plane. With this choice of geometry, the linear polarization of the subsequent emission within electric dipole approximation can be written as [34]

$$P = \frac{(-1)^{J_0+2J_b} \sqrt{\frac{27}{8}} \frac{(2J_b+1)}{\sigma(\alpha_b J_b)} \left\{ \begin{matrix} 1 & 1 & 2 \\ J_b & J_b & J_0 \end{matrix} \right\} \sum_{M_b} (-1)^{M_b} \langle J_b M_b \quad J_b - M_b | 2 0 \rangle \sigma(\alpha_b J_b M_b)}{1 + (-1)^{J_0+2J_b} \sqrt{\frac{3}{8}} \frac{(2J_b+1)}{\sigma(\alpha_b J_b)} \left\{ \begin{matrix} 1 & 1 & 2 \\ J_b & J_b & J_0 \end{matrix} \right\} \sum_{M_b} (-1)^{M_b} \langle J_b M_b \quad J_b - M_b | 2 0 \rangle \sigma(\alpha_b J_b M_b)} \quad (5)$$

We have simplified the above expression for various dipole allowed transitions for the L- and M-shell excitations of the tungsten ions considered in our earlier [25–27] as well as in the present work. For sake of convenience to the readers, all these formulae are compiled in Table 1 for the various decay transitions between states J_b to J_0 . Here, the lower state $|\alpha_0 J_0\rangle$ is the same as considered for electron impact excitation *i.e.*, $|\alpha_a J_a\rangle$.

Table 1. Degree of linear polarization of the emitted photon for transition $J_b \rightarrow J_0$ in terms of magnetic sublevel cross-sections (σ_{M_b}).

Transition $J_b \rightarrow J_0$	Polarization, P	Transition $J_b \rightarrow J_0$	Polarization, P
1→0	$\frac{\sigma_0 - \sigma_1}{\sigma_0 + \sigma_1}$	3/2→1/2	$\frac{3(\sigma_{1/2} - \sigma_{3/2})}{3\sigma_{3/2} + 5\sigma_{1/2}}$
1→2	$\frac{\sigma_0 - \sigma_1}{7\sigma_0 + 13\sigma_1}$	3/2→3/2	$\frac{3(\sigma_{1/2} - \sigma_{3/2})}{6\sigma_{3/2} + 4\sigma_{1/2}}$
2→1	$\frac{3(2\sigma_2 - \sigma_1 - \sigma_0)}{6\sigma_2 + 9\sigma_1 + 5\sigma_0}$	3/2→5/2	$\frac{3(\sigma_{1/2} - \sigma_{3/2})}{19\sigma_{3/2} + 21\sigma_{1/2}}$
2→2	$\frac{3(2\sigma_2 - \sigma_1 - \sigma_0)}{10\sigma_2 + 7\sigma_1 + 3\sigma_0}$	5/2→3/2	$\frac{(5\sigma_{5/2} - \sigma_{3/2} - 4\sigma_{1/2})}{5\sigma_{5/2} + 7\sigma_{3/2} + 8\sigma_{1/2}}$

Table 1. Cont.

Transitio $n J_b \rightarrow J_0$	Polarization, P	Transition $J_b \rightarrow J_0$	Polarization, P
2→3	$\frac{-3(2\sigma_2 - \sigma_1 - \sigma_0)}{26\sigma_2 + 29\sigma_1 + 15\sigma_0}$	5/2→5/2	$\frac{2(5\sigma_{5/2} - \sigma_{3/2} - 4\sigma_{1/2})}{15\sigma_{5/2} + 11\sigma_{3/2} + 9\sigma_{1/2}}$
3→2	$\frac{-3(5\sigma_3 - 3\sigma_1 - 2\sigma_0)}{15\sigma_3 + 20\sigma_2 + 23\sigma_1 + 12\sigma_0}$	7/2→5/2	$\frac{3(7\sigma_{7/2} + \sigma_{5/2} - 3\sigma_{3/2} - 5\sigma_{1/2})}{21\sigma_{7/2} + 27\sigma_{5/2} + 31\sigma_{3/2} + 33\sigma_{1/2}}$
3→3	$\frac{3(5\sigma_3 - 3\sigma_1 - 2\sigma_0)}{21\sigma_3 + 16\sigma_2 + 13\sigma_1 + 6\sigma_0}$	7/2→9/2	$\frac{-3(7\sigma_{7/2} + \sigma_{5/2} - 3\sigma_{3/2} - 5\sigma_{1/2})}{53\sigma_{7/2} + 59\sigma_{5/2} + 63\sigma_{3/2} + 65\sigma_{1/2}}$
3→4	$\frac{-3(5\sigma_3 - 3\sigma_1 - 2\sigma_0)}{43\sigma_3 + 48\sigma_2 + 51\sigma_1 + 26\sigma_0}$	9/2→9/2	$\frac{3(12\sigma_{9/2} + 4\sigma_{7/2} - 2\sigma_{5/2} - 6\sigma_{3/2} - 8\sigma_{1/2})}{45\sigma_{9/2} + 37\sigma_{7/2} + 31\sigma_{5/2} + 27\sigma_{3/2} + 25\sigma_{1/2}}$
4→3	$\frac{-(28\sigma_4 + 7\sigma_3 - 8\sigma_2 - 17\sigma_1 - 10\sigma_0)}{28\sigma_4 + 35\sigma_3 + 40\sigma_2 + 43\sigma_1 + 22\sigma_0}$	11/2→11/2	$\frac{55\sigma_{11/2} + 25\sigma_{9/2} + \sigma_{7/2} - 17\sigma_{5/2} - 29\sigma_{3/2} - 35\sigma_{1/2}}{66\sigma_{11/2} + 56\sigma_{9/2} + 48\sigma_{7/2} + 42\sigma_{5/2} + 38\sigma_{3/2} + 36\sigma_{1/2}}$
4→4	$\frac{28\sigma_4 + 7\sigma_3 - 8\sigma_2 - 17\sigma_1 - 10\sigma_0}{36\sigma_4 + 29\sigma_3 + 24\sigma_2 + 21\sigma_1 + 10\sigma_0}$	5→4	$\frac{-3(15\sigma_5 + 6\sigma_4 - \sigma_3 - 6\sigma_2 - 9\sigma_1 - 5\sigma_0)}{45\sigma_5 + 54\sigma_4 + 61\sigma_3 + 66\sigma_2 + 69\sigma_1 + 35\sigma_0}$
6→6	$\frac{3(22\sigma_6 + 11\sigma_5 + 2\sigma_4 - 5\sigma_3 - 10\sigma_2 - 13\sigma_1 - 7\sigma_0)}{78\sigma_6 + 67\sigma_5 + 58\sigma_4 + 51\sigma_3 + 46\sigma_2 + 43\sigma_1 + 21\sigma_0}$		

3. Brief Review of the Earlier Work

In the following subsections we have given the review of our work along with other earlier work carried out for electron impact L- and M-shell excitations in various charged states of tungsten W^{n+} ($n = 44-66$) ions [25–27].

3.1. L-Shell Excitation of Mg- through O-like Tungsten Ions

There have been continuous efforts to investigate emission spectra of highly charged Mg-like through O-like tungsten ions. Beiersdorfer *et al* [21] reported high-resolution crystal spectroscopy measurements and identified ten lines in neon-like W^{64+} arising due to the $n = 3 \rightarrow n = 2$ L-shell X-ray transitions as well as inner-shell collisional satellite lines associated with oxygen-like W^{66+} , fluorine-like W^{65+} , sodium-like W^{63+} , and magnesium-like W^{62+} ions. In this work, they have also calculated the transition energies by using flexible atomic code (FAC). A great deal of other theoretical calculations reported for $W^{62+}-W^{66+}$ ions, mainly focused on computation of excitation energies, oscillator strengths and transition probabilities [35–39]. However, Zhang and co-workers [40–43] reported relativistic distorted wave calculations for electron excitation cross-sections of Na-like through O-like tungsten ions.

We performed relativistic distorted wave calculations for the L-shell electron excitations of Mg-like W^{62+} through O-like W^{66+} ions [26]. The ground state configurations of these ions are $(1s^2 2s^2 2p^6 3s^2)_J=0$ for Mg-like, $(1s^2 2s^2 2p^6 3s)_J=1/2$ for Na-like, $(1s^2 2s^2 2p^6)_J=0$ for Ne-like, $(1s^2 2s^2 2p^5)_J=3/2$ for F-like and $(1s^2 2s^2 2p^4)_J=2$ for O-like tungsten ions. Excitations were considered from inner $2p$ shell to $3d$ orbital for Mg-like W^{62+} and Na-like W^{63+} ions. In case of W^{63+} ion double excitations leading to double occupancy in $3p$ orbital and vacancies in $2p$ and $3s$ orbitals have also been considered. For Ne-like W^{64+} and F-like W^{65+} ions, excitation of their ground states to the states with a hole in $n = 2$ level and promotion of one

electron to the $n = 3$ level was considered. In case of the O-like W^{66+} ion, a number of transitions between levels with $n = 2$ and $n = 3$ were investigated. The list of all the transitions considered is given in Table 2.

Table 2. L-shell excitations considered in Mg-like W^{62+} through O-like W^{66+} ions [26].

Mg-like W^{62+} Ion		Na-like W^{63+} Ion		Ne-like W^{64+} Ion	
Lower Level	Upper Level	Lower Level	Upper Level	Lower Level	Upper Level
				$(2p^6)_{J=0}$	$(2s^2 2p_{3/2}^5 3s_{1/2})_{J=2}$
				$(2p^6)_{J=0}$	$(2s^2 2p_{3/2}^5 3s_{1/2})_{J=1}$
			$(2p_{3/2}^5 3s_{1/2} 3d_{5/2})_{J=3/2}$	$(2p^6)_{J=0}$	$(2s^2 2p_{3/2}^5 3p_{1/2})_{J=2}$
			$(2p_{3/2}^5 3s_{1/2} 3d_{5/2})_{J=1/2}$	$(2p^6)_{J=0}$	$(2s^2 2p_{3/2}^5 3d_{3/2})_{J=1}$
$(2p^6 3s^2)_{J=0}$	$(2p_{3/2}^5 3s^2 3d_{5/2})_{J=1}$	$(2p^6 3s)_{J=1/2}$	$(2p_{1/2}^5 3p_{1/2} 3p_{3/2})_{J=3/2}$	$(2p^6)_{J=0}$	$(2s^2 2p_{3/2}^5 3d_{5/2})_{J=1}$
$(2p^6 3s^2)_{J=0}$	$(2p_{1/2}^5 3s^2 3d_{3/2})_{J=1}$	$(2p^6 3s)_{J=1/2}$	$(2p_{1/2}^5 3s_{1/2} 3d_{3/2})_{J=1/2}$	$(2p^6)_{J=0}$	$(2s^2 2p_{1/2}^5 3s_{1/2})_{J=1}$
			$(2p_{1/2}^5 3s_{1/2} 3d_{3/2})_{J=3/2}$	$(2p^6)_{J=0}$	$(2s_{1/2} 2p^6 3p_{1/2})_{J=1}$
				$(2p^6)_{J=0}$	$(2s^2 2p_{1/2}^5 3d_{3/2})_{J=1}$
				$(2p^6)_{J=0}$	$(2s_{1/2} 2p^6 3p_{3/2})_{J=1}$
				$(2p^6)_{J=0}$	$(2s_{1/2} 2p^6 3d_{5/2})_{J=2}$
F-like W^{65+} Ion		O-like W^{66+} Ion			
Lower Level	Upper Level	Lower Level	Upper Level		
$(2p_{3/2}^5)_{J=3/2}$	$(2p_{1/2}^2 2p_{3/2}^2 3s_{1/2})_{J=5/2}$	$(2s_{1/2} 2p_{1/2}^2 2p_{3/2}^3)_{J=2}$	$(2s^2 2p_{1/2} 2p_{3/2}^2 3p_{1/2})_{J=2}$		
$(2p_{3/2}^5)_{J=3/2}$	$(2p_{1/2}^2 2p_{3/2}^2 3s_{1/2})_{J=3/2}$	$(2s^2 2p_{1/2}^2 2p_{3/2}^2)_{J=0}$	$(2s^2 2p_{1/2}^2 2p_{3/2} 3s_{1/2})_{J=1}$		
$(2p_{3/2}^5)_{J=3/2}$	$(2p_{1/2}^2 2p_{3/2}^2 3s_{1/2})_{J=1/2}$	$(2s_{1/2} 2p_{1/2}^2 2p_{3/2}^3)_{J=2}$	$(2s_{1/2} 2p_{1/2}^2 2p_{3/2}^2 3s_{1/2})_{J=2} (1)^b$		
$(2p_{3/2}^5)_{J=3/2}$	$(2p_{1/2}^2 2p_{3/2}^2 3p_{1/2})_{J=5/2}$	$(2s_{1/2} 2p_{1/2}^2 2p_{3/2}^3)_{J=1}$	$(2s_{1/2} 2p_{1/2}^2 2p_{3/2}^2 3s_{1/2})_{J=2} (2)^b$		
$(2p_{3/2}^5)_{J=3/2}$	$(2p_{1/2}^2 2p_{3/2}^2 3p_{1/2})_{J=3/2}$	$(2s^2 2p_{1/2}^2 2p_{3/2}^2)_{J=2}$	$(2s^2 2p_{1/2}^2 2p_{3/2} 3s_{1/2})_{J=2}$		
$(2p_{3/2}^5)_{J=3/2}$	$(2p_{1/2}^2 2p_{3/2}^2 3d_{5/2})_{J=5/2} (1)^a$	$(2s^2 2p_{1/2}^2 2p_{3/2}^2)_{J=2}$	$(2s^2 2p_{1/2}^2 2p_{3/2} 3s_{1/2})_{J=1}$		
$(2p_{3/2}^5)_{J=3/2}$	$(2p_{1/2}^2 2p_{3/2}^2 3d_{5/2})_{J=3/2}$	$(2s^2 2p_{1/2}^2 2p_{3/2}^2)_{J=2}$	$(2s^2 2p_{1/2}^2 2p_{3/2} 3d_{5/2})_{J=2}$		
$(2p_{3/2}^5)_{J=3/2}$	$(2p_{1/2}^2 2p_{3/2}^2 3d_{5/2})_{J=5/2} (2)^a$	$(2s^2 2p_{1/2}^2 2p_{3/2}^2)_{J=2}$	$(2s^2 2p_{1/2}^2 2p_{3/2} 3d_{5/2})_{J=3}$		
$(2p_{3/2}^5)_{J=3/2}$	$(2p_{1/2} 2p_{3/2}^3 3d_{3/2})_{J=1/2}$	$(2s^2 2p_{1/2}^2 2p_{3/2}^2)_{J=2}$	$(2s^2 2p_{1/2} 2p_{3/2}^2 3d_{3/2})_{J=3}$		
$(2p_{3/2}^5)_{J=3/2}$	$(2p_{1/2} 2p_{3/2}^3 3d_{3/2})_{J=5/2}$	$(2s^2 2p_{1/2}^2 2p_{3/2}^2)_{J=2}$	$(2s^2 2p_{1/2} 2p_{3/2}^2 3d_{3/2})_{J=2}$		
$(2p_{3/2}^5)_{J=3/2}$	$(2p_{1/2} 2p_{3/2}^3 3d_{3/2})_{J=3/2}$	$(2s^2 2p_{1/2}^2 2p_{3/2}^2)_{J=2}$	$(2s^2 2p_{1/2} 2p_{3/2}^2 3d_{3/2})_{J=1}$		

^{a, b} Number 1 or 2 inside the parenthesis refers the two different states with same value of J .

The ground as well as excited states of these ions were expressed within the multi-configuration Dirac-Fock (MCDF) approach as linear combination of other configuration state wavefunctions having the same total angular momentum J and parity. For this purpose we used GRASP2k code [33] and calculated excitation energies and dipole oscillator strengths associated with the transitions listed in Table 2. These values were compared with the measurements on excitation energies reported by Beiersdorfer *et al.* [21] as well as available theoretical results [21,35–40,42]. In particular, we found that

the maximum deviation of excitation energy was 0.029% for Mg-like, 0.056% for Na-like, 0.079% for Ne-like and F-like and 0.049% for O-like tungsten ions with the measured and the other available theoretical values. Electron impact L-shell excitation cross-sections were obtained in the range of the incident electron energies from threshold to 60 keV. We compared our results with the available other RDW calculations for Ne-like W^{64+} [40] and F-like W^{63+} [42] ions and found good agreement. We also observed that a transition involving double excitation yielded lesser cross-sections as compared to a single electron excitation. This is due to the fact that for double excitation direct T -matrix is zero and only the exchange T -matrix contributes. We further carried out analytical fitting of our calculated cross-section data for each transition in the entire range of the incident electron energy so that the cross-section at any desired energy can be readily obtained and the expression of analytic fit can be directly used in any plasma model.

In addition to the excitation cross-sections, we also calculated the polarization of the subsequently emitted photon from the L-shell excited transitions by using the suitable relation from Table 1 for a particular decay transition. In general, we observed a similar behavior of the polarization for all the considered transitions *i.e.*, the polarization first increased with an increase in energy and reached its maximum value for the incident energy at approximately two times the threshold energy and then started to decrease with the increase of electron energy [26].

3.2. M-Shell Excitation of W^{n+} Tungsten Ions

3.2.1. Excitation of Co-like through Zn-like Tungsten Ions

The growing interest to understand tungsten ions spectra for diagnostics of fusion plasma makes the study of their M-shell spectra amenable. Therefore, a significant amount of theoretical [25,27,44–46] and experimental [14,17–20,22] work has been performed on M-shell spectra of various ion charge species of tungsten. In this context, Clementson *et al.* [18] have measured the M-shell spectra of Zn-like W^{44+} through Co-like W^{47+} ions using an X-ray calorimeter spectrometer at the SuperEBIT. They studied spectra at excitation energies 3.3, 4.0 and 4.1 keV and observed strong line emission in the 1500–3600 eV soft X-ray range. Clementson *et al.* [18] also utilized FAC code to carry out relativistic atomic structure and collisional-radiative calculations and compared their calculated and observed spectra. For the electron impact excitation studies of these ions, Zhang *et al.* [44,45] reported their relativistic distorted wave collision strengths for Ni-like and Cu-like tungsten ions. Recently, Xie *et al.* [46] reported magnetic sublevel excitation cross-sections and polarization of Ni-like through Ge-like tungsten ions.

Though one can find a great deal of scattered literature on different ionic stages of tungsten ions, the existing electron impact excitation cross-section data is still insufficient. In the light of M-shell spectra of Zn-like to Co-like W ions as observed by Clementson *et al.* [18], we undertook the task of extensive cross-section calculations for M-shell excitations in these ions. Using the RDW method we studied the excitation of the electrons from $3d$ to $4p$ and n_f sub-shells where $n = 4–6$ for Zn-like W^{44+} and Cu-like W^{45+} , $n = 4–8$ for Ni-like W^{46+} and $n = 4$ and 5 for Co-like W^{47+} [25]. We selected all the dipole allowed transitions as listed in Table 3, which belong to the most intense lines reported in the measured spectra [18]. For all these transitions, excitation energies and oscillator strengths were calculated using GRASP92 code of Parpia *et al.* [32]. These values were in good agreement with the measurements [18] and other

relativistic theories [45,47]. For example, our calculated excitation energies differed from the measured values by 0.20% for Zn-like, 0.23% for Cu-like, 0.13% for Ni-like and 0.29% for Co-like tungsten ions.

Table 3. M-shell excitations from the ground state of Zn-like W^{44+} through Co-like W^{47+} ions [25].

Ion	Zn-like W^{44+}	Cu-like W^{45+}	Ni-like W^{46+}	Co-like W^{47+}
Ground state	$(3\bar{d}^4 3d^6 4s^2)_{J=0}$	$(3\bar{d}^4 3d^6 4s)_{J=1/2}$	$(3\bar{d}^4 3d^6)_{J=0}$	$(3\bar{d}^4 3d^5)_{J=5/2}$
Excited States	$(3\bar{d}^3 3d^6 4s^2 4\bar{p})_{J=1}$	$(3\bar{d}^3 3d^6 4s4\bar{p})_{J=3/2}$	$(3\bar{d}^4 3d^5 4p)_{J=1}$	$(3\bar{d}^3 3d^5 4\bar{p})_{J=7/2}$
	$(3\bar{d}^4 3d^5 4s^2 4\bar{f})_{J=1}$	$(3\bar{d}^3 3d^6 4s4\bar{p})_{J=1/2}$	$(3\bar{d}^3 3d^6 4p)_{J=1}$	$(3\bar{d}^3 3d^5 4\bar{p})_{J=3/2}$
	$(3\bar{d}^3 3d^6 4s^2 4\bar{f})_{J=1}$	$(3\bar{d}^4 3d^5 4s4p)_{J=3/2}$	$(3\bar{d}^4 3d^5 4f)_{J=1}$	$(3\bar{d}^4 3d^4 4p)_{J=7/2}$
	$(3\bar{d}^4 3d^5 4s^2 5\bar{f})_{J=1}$	$(3\bar{d}^3 3d^6 4s4p)_{J=1/2}$ (1) [#]	$(3\bar{d}^3 3d^6 4\bar{f})_{J=1}$	$(3\bar{d}^4 3d^4 4p)_{J=5/2}$ (1) [*]
	$(3\bar{d}^4 3d^5 4s^2 6\bar{f})_{J=1}$	$(3\bar{d}^3 3d^6 4s4p)_{J=3/2}$	$(3\bar{d}^4 3d^5 5\bar{f})_{J=1}$	$(3\bar{d}^4 3d^4 4p)_{J=5/2}$ (2) [*]
	$(3\bar{d}^3 3d^6 4s^2 6\bar{f})_{J=1}$	$(3\bar{d}^3 3d^6 4s4p)_{J=1/2}$ (2) [#]	$(3\bar{d}^3 3d^6 5\bar{f})_{J=1}$	$(3\bar{d}^4 3d^4 4p)_{J=3/2}$
		$(3\bar{d}^4 3d^5 4s4\bar{f})_{J=3/2}$	$(3\bar{d}^4 3d^5 6\bar{f})_{J=1}$	$(3\bar{d}^4 3d^4 4\bar{f})_{J=5/2}$ (1) ^{**}
		$(3\bar{d}^4 3d^5 4s4\bar{f})_{J=1/2}$	$(3\bar{d}^3 3d^6 6\bar{f})_{J=1}$	$(3\bar{d}^4 3d^4 4\bar{f})_{J=7/2}$
		$(3\bar{d}^3 3d^6 4s4\bar{f})_{J=1/2}$	$(3\bar{d}^4 3d^5 7\bar{f})_{J=1}$	$(3\bar{d}^4 3d^4 4\bar{f})_{J=3/2}$
		$(3\bar{d}^3 3d^6 4s4\bar{f})_{J=3/2}$	$(3\bar{d}^3 3d^6 7\bar{f})_{J=1}$	$(3\bar{d}^4 3d^4 4f)_{J=7/2}$ (1) ⁺
		$(3\bar{d}^4 3d^5 4s^1 5\bar{f})_{J=1/2}$	$(3\bar{d}^4 3d^5 8\bar{f})_{J=1}$	$(3\bar{d}^4 3d^4 4f)_{J=5/2}$ (1) ⁺⁺
		$(3\bar{d}^4 3d^5 4s5\bar{f})_{J=3/2}$	$(3\bar{d}^3 3d^6 8\bar{f})_{J=1}$	$(3\bar{d}^4 3d^4 4f)_{J=3/2}$
		$(3\bar{d}^3 3d^6 4s5\bar{f})_{J=1/2}$		$(3\bar{d}^4 3d^4 4f)_{J=5/2}$ (2) ⁺⁺
		$(3\bar{d}^3 3d^6 4s5\bar{f})_{J=3/2}$		$(3\bar{d}^4 3d^4 4f)_{J=7/2}$ (2) ⁺
		$(3\bar{d}^4 3d^5 4s6\bar{f})_{J=1/2}$		$(3\bar{d}^4 3d^4 4\bar{f})_{J=5/2}$ (2) ^{**}
		$(3\bar{d}^4 3d^5 4s6\bar{f})_{J=3/2}$		$(3\bar{d}^3 3d^5 4\bar{f})_{J=3/2}$
		$(3\bar{d}^3 3d^6 4s6\bar{f})_{J=3/2}$		$(3\bar{d}^3 3d^5 4f)_{J=5/2}$
		$(3\bar{d}^3 3d^6 4s6\bar{f})_{J=1/2}$		$(3\bar{d}^3 3d^5 4\bar{f})_{J=7/2}$
				$(3\bar{d}^3 3d^5 4\bar{f})_{J=5/2}$
				$(3\bar{d}^4 3d^4 5\bar{f})_{J=5/2}$
			$(3\bar{d}^4 3d^4 5f)_{J=7/2}$	
			$(3\bar{d}^3 3d^5 5\bar{f})_{J=3/2}$	
			$(3\bar{d}^3 3d^5 5\bar{f})_{J=7/2}$	
			$(3\bar{d}^3 3d^5 5\bar{f})_{J=5/2}$	

^{#,*,**,+,++} Number 1 or 2 inside the parenthesis refers the two different states with same value of J .

Cross-sections for all the above-mentioned M-shell transitions listed in Table 3 were calculated in the wide range of incident electron energy up to 50 keV. We found that the cross-sections for excitation of an electron from $3d$ or $3\bar{d}$ to nf or $n\bar{f}$ decreased as Δn increased. Thus, it was as expected that the increase in excitation energy would lead to a decrease in cross-section values. We also compared our cross-sections for the transitions $3\bar{d} \rightarrow 4p$, $3d \rightarrow 4p$, $3\bar{d} \rightarrow 4\bar{f}$ and $3d \rightarrow 4f$ for Ni-like W^{46+} ions with the

available RDW calculations of Zhang *et al.* [45] at energies up to 12 keV only. Good agreement of our results with the calculations of Zhang *et al.* [45] was found which indicates the consistency and reliability of both the calculations. We have also provided the analytic fitting parameters as we did for L-shell excitations, so that analytic fit can be implemented directly in any plasma model and a cross-section can be calculated at any energy.

Further, polarization of the photons emitted after decay of the M-shell excited ionic states was calculated using the different magnetic sublevel cross-sections. We noticed again that the polarization initially increased with increasing electron energy and showed a broad peak near threshold before decreasing rapidly at higher incident electron energies. In case of Cu-like and Zn-like tungsten ions, polarization values for the photon decay due to deexcitation of one electron to $3d$ and $3\bar{d}$ from $4p$ and $4\bar{p}$ orbitals were greater than those from nf and $n\bar{f}$ orbitals. Another interesting feature noticed for all four ions was that the polarization of photons associated with decay transitions *viz.* $n\bar{f} \rightarrow 3\bar{d}$ and $nf \rightarrow 3d$ was nearly equal for a given value of n .

3.2.2. Excitation of Fe-like through Al-like Tungsten Ions

We also applied the RDW theory to study M-shell excitation *viz.* $3p_{3/2}-3d_{5/2}$ in Fe-like through Al-like tungsten ions [27]. This work was undertaken in view of the recent spectral measurements of wavelengths in the 27–41 Å range for Fe-like through Al-like tungsten ions by Lennartsson *et al* [22] at Livermore EBIT-I. A number of theoretical and experimental investigations have been reported for M-shell transitions in these 14 tungsten ions.

All the transitions considered for these ions are listed in Table 4. We calculated the excitation energies and oscillator strengths for these transitions and compared them with the values reported earlier [22,48–55]. We observed overall good agreement with the experimental and other theoretical results. We also found that our calculated excitation energies were within 1% of the measurements and the FAC results. Further, utilizing the target ion wavefunctions, we calculated RDW cross-sections for the transitions given in Table 4. It was observed [27] that cross-sections corresponding to the transition $J_a = 0$ to $J_b = 1$ were maximal for a given ion. As expected, the relative values of cross-sections in a particular ion were governed by the values of oscillator strengths *i.e.*, transition with greater value of oscillator strength yielded more cross-sections. Furthermore, analytic fitting of the cross-sections was done and fitting coefficients were provided for plasma modeling.

We also performed the analysis of the linear polarization of photons which is expressible in terms of magnetic sublevel cross-sections of the excited state as given in Table 1. We observed that decay of $J_b = 1$ to $J_0 = 0$ state resulted in maximum polarization near threshold of all the transitions considered. Moreover, the transitions leading to $\Delta J = -1$ caused emission of feebly polarized photons with maximal values of only 2%. In general, photons emitted due to transitions with $\Delta J = 0$ were more strongly polarized than those with $\Delta J = 1$.

Table 4. M-shell excitations considered in Fe-like W^{48+} through Al-like W^{61+} ions [27].

W^{48+}		W^{49+}	
<i>Lower Level</i>	<i>Upper Level</i>	<i>Lower Level</i>	<i>Upper Level</i>
$[(3p^6 3d_{3/2}^4)_0 3d_{5/2}^4]_{J=4}$	$[(3p_{1/2}^2 3p_{3/2}^3 3d_{3/2}^4)_{3/2} 3d_{5/2}^5]_{J=3}$	$[(3p^6 3d_{3/2}^4)_0 3d_{5/2}^3]_{J=9/2}$	$[(3p_{1/2}^2 3p_{3/2}^3 3d_{3/2}^4)_{3/2} (3d_{5/2}^4)_4]_{J=7/2}$
$[(3p^6 3d_{3/2}^4)_0 3d_{5/2}^4]_{J=0}$	$[(3p_{1/2}^2 3p_{3/2}^3 3d_{3/2}^4)_{3/2} 3d_{5/2}^5]_{J=1}$	$[(3p^6 3d_{3/2}^4)_0 3d_{5/2}^3]_{J=5/2}$	$[(3p_{1/2}^2 3p_{3/2}^3 3d_{3/2}^4)_{3/2} (3d_{5/2}^4)_2]_{J=3/2}$
$[(3p^6 3d_{3/2}^4)_0 3d_{5/2}^4]_{J=2}$	$[(3p_{1/2}^2 3p_{3/2}^3 3d_{3/2}^4)_{3/2} 3d_{5/2}^5]_{J=2}$	$[(3p^6 3d_{3/2}^4)_0 3d_{5/2}^3]_{J=5/2}$	$[(3p_{1/2}^2 3p_{3/2}^3 3d_{3/2}^4)_{3/2} (3d_{5/2}^4)_4]_{J=5/2}$
$[(3p^6 3d_{3/2}^4)_0 3d_{5/2}^4]_{J=4}$	$[(3p_{1/2}^2 3p_{3/2}^3 3d_{3/2}^4)_{3/2} 3d_{5/2}^5]_{J=4}$	$[(3p^6 3d_{3/2}^4)_0 3d_{5/2}^3]_{J=9/2}$	$[(3p_{1/2}^2 3p_{3/2}^3 3d_{3/2}^4)_{3/2} (3d_{5/2}^4)_4]_{J=9/2}$
		$[(3p^6 3d_{3/2}^4)_0 3d_{5/2}^3]_{J=5/2}$	$[(3p_{1/2}^2 3p_{3/2}^3 3d_{3/2}^4)_{3/2} (3d_{5/2}^4)_2]_{J=7/2}$
W^{50+}		W^{51+}	
<i>Lower Level</i>	<i>Upper Level</i>	<i>Lower Level</i>	<i>Upper Level</i>
$[(3p^6 3d_{3/2}^4)_0 3d_{5/2}^2]_{J=4}$	$[(3p_{1/2}^2 3p_{3/2}^3 3d_{3/2}^4)_{3/2} (3d_{5/2}^3)_{9/2}]_{J=4}$	$[(3p^6 3d_{3/2}^4)_0 3d_{5/2}^2]_{J=5/2}$	$[(3p_{1/2}^2 3p_{3/2}^3 3d_{3/2}^4)_{3/2} (3d_{5/2}^3)_4]_{J=5/2}$
$[(3p^6 3d_{3/2}^4)_0 3d_{5/2}^2]_{J=4}$	$[(3p_{1/2}^2 3p_{3/2}^3 3d_{3/2}^4)_{3/2} (3d_{5/2}^3)_{5/2}]_{J=3}$	$[(3p^6 3d_{3/2}^4)_0 3d_{5/2}^2]_{J=5/2}$	$[(3p_{1/2}^2 3p_{3/2}^3 3d_{3/2}^4)_{3/2} (3d_{5/2}^3)_4]_{J=7/2}$
$[(3p^6 3d_{3/2}^4)_0 3d_{5/2}^2]_{J=2}$	$[(3p_{1/2}^2 3p_{3/2}^3 3d_{3/2}^4)_{3/2} (3d_{5/2}^3)_{3/2}]_{J=1}$	$[(3p^6 3d_{3/2}^4)_0 3d_{5/2}^2]_{J=5/2}$	$[(3p_{1/2}^2 3p_{3/2}^3 3d_{3/2}^4)_{3/2} (3d_{5/2}^3)_2]_{J=7/2}$
$[(3p^6 3d_{3/2}^4)_0 3d_{5/2}^2]_{J=2}$	$[(3p_{1/2}^2 3p_{3/2}^3 3d_{3/2}^4)_{3/2} (3d_{5/2}^3)_{5/2}]_{J=3}$	$[(3p^6 3d_{3/2}^4)_{3/2} 3d_{5/2}^2]_{J=1/2}$	$[(3p_{1/2}^2 3p_{3/2}^3 3d_{3/2}^4)_{3/2} (3d_{5/2}^3)_{9/2}]_{J=11/2}$
$[(3p^6 3d_{3/2}^4)_0 3d_{5/2}^2]_{J=2}$	$[(3p_{1/2}^2 3p_{3/2}^3 3d_{3/2}^4)_{3/2} (3d_{5/2}^3)_{5/2}]_{J=3}$		
$[(3p^6 3d_{3/2}^4)_{3/2} 3d_{9/2}^2]_{J=6}$	$[(3p_{1/2}^2 3p_{3/2}^3 3d_{3/2}^4)_{3/2} (3d_{5/2}^3)_4]_{J=6}$	W^{52+}	
$[(3p^6 3d_{3/2}^4)_0 3d_{5/2}^2]_{J=2}$	$[(3p_{1/2}^2 3p_{3/2}^3 3d_{3/2}^4)_{3/2} (3d_{5/2}^3)_{5/2}]_{J=2}$	<i>Lower Level</i>	<i>Upper Level</i>
$[(3p^6 3d_{3/2}^4)_0 3d_{5/2}^2]_{J=4}$	$[(3p_{1/2}^2 3p_{3/2}^3 3d_{3/2}^4)_{3/2} (3d_{5/2}^3)_{9/2}]_{J=5}$	$[3p^6 3d_{3/2}^4]_{J=0}$	$[(3p_{1/2}^2 3p_{3/2}^3 3d_{3/2}^4)_{3/2} 3d_{5/2}^2]_{J=1}$
		$[(3p^6 3d_{3/2}^4)_{3/2} 3d_{5/2}^2]_{J=3}$	$[(3p_{1/2}^2 3p_{3/2}^3 3d_{3/2}^4)_{3/2} (3d_{5/2}^3)_2]_{J=2}$
		$[(3p^6 3d_{3/2}^4)_{3/2} 3d_{5/2}^2]_{J=3}$	$[(3p_{1/2}^2 3p_{3/2}^3 3d_{3/2}^4)_{3/2} (3d_{5/2}^3)_2]_{J=3}$
		$[(3p^6 3d_{3/2}^4)_{3/2} 3d_{5/2}^2]_{J=4}$	$[(3p_{1/2}^2 3p_{3/2}^3 3d_{3/2}^4)_{3/2} (3d_{5/2}^3)_4]_{J=5}$
		$[(3p^6 3d_{3/2}^4)_{3/2} 3d_{5/2}^2]_{J=3}$	$[(3p_{1/2}^2 3p_{3/2}^3 3d_{3/2}^4)_{3/2} (3d_{5/2}^3)_4]_{J=4}$
		$[(3p^6 3d_{3/2}^4)_{3/2} 3d_{5/2}^2]_{J=4}$	$[(3p_{1/2}^2 3p_{3/2}^3 3d_{3/2}^4)_{3/2} (3d_{5/2}^3)_3]_{J=5}$
W^{53+}		W^{55+}	
<i>Lower Level</i>	<i>Upper Level</i>	<i>Lower Level</i>	<i>Upper Level</i>
$[3p^6 3d_{3/2}^3]_{J=3/2}$	$[(3p_{1/2}^2 3p_{3/2}^3 3d_{3/2}^3)_3 3d_{5/2}^2]_{J=3/2}$		
$[3p^6 3d_{3/2}^3]_{J=3/2}$	$[(3p_{1/2}^2 3p_{3/2}^3 3d_{3/2}^3)_2 3d_{5/2}^2]_{J=5/2}$		
$[3p^6 3d_{3/2}^3]_{J=3/2}$	$[(3p_{1/2}^2 3p_{3/2}^3 3d_{3/2}^3)_3 3d_{5/2}^2]_{J=1/2}$		
W^{54+}		W^{55+}	
<i>Lower Level</i>	<i>Upper Level</i>	<i>Lower Level</i>	<i>Upper Level</i>
$[3p^6 3d_{3/2}^2]_{J=2}$	$[(3p_{1/2}^2 3p_{3/2}^3)_{3/2} (3d_{3/2}^2)_2]_{3/2} 3d_{5/2}^2]_{J=3}$		
$[3p^6 3d_{3/2}^2]_{J=2}$	$[(3p_{1/2}^2 3p_{3/2}^3)_{3/2} (3d_{3/2}^2)_2]_{7/2} 3d_{5/2}^2]_{J=2}$		
$[3p^6 3d_{3/2}^2]_{J=2}$	$[(3p_{1/2}^2 3p_{3/2}^3)_{3/2} (3d_{3/2}^2)_2]_{7/2} 3d_{5/2}^2]_{J=1}$	$[3p^6 3d_{3/2}^2]_{J=3/2}$	$[(3p_{1/2}^2 3p_{3/2}^3 3d_{3/2}^2)_2 3d_{5/2}^2]_{J=5/2}$
$[3p^6 3d_{3/2}^2]_{J=2}$	$[(3p_{1/2}^2 3p_{3/2}^3)_{3/2} (3d_{3/2}^2)_0]_{3/2} 3d_{5/2}^2]_{J=1}$	$[3p^6 3d_{3/2}^2]_{J=3/2}$	$[(3p_{1/2}^2 3p_{3/2}^3 3d_{3/2}^2)_3 3d_{5/2}^2]_{J=3/2}$
$[3p^6 3d_{3/2}^2]_{J=0}$	$[(3p_{1/2}^2 3p_{3/2}^3)_{3/2} (3d_{3/2}^2)_0]_{3/2} 3d_{5/2}^2]_{J=1}$	$[3p^6 3d_{3/2}^2]_{J=3/2}$	$[(3p_{1/2}^2 3p_{3/2}^3)_{3/2} 3d_{3/2}^2]_{3/2} 3d_{5/2}^2]_{J=1/2}$
$[3p^6 3d_{3/2}^2]_{J=2}$	$[(3p_{1/2}^2 3p_{3/2}^3)_{3/2} (3d_{3/2}^2)_0]_{3/2} 3d_{5/2}^2]_{J=3}$	$[3p^6 3d_{3/2}^2]_{J=3/2}$	$[(3p_{1/2}^2 3p_{3/2}^3)_{3/2} 3d_{3/2}^2]_{3/2} 3d_{5/2}^2]_{J=5/2}$
$[3p^6 3d_{3/2}^2]_{J=2}$	$[(3p_{1/2}^2 3p_{3/2}^3)_{3/2} (3d_{3/2}^2)_0]_{3/2} 3d_{5/2}^2]_{J=2}$		
W^{56+}		W^{57+}	
<i>Lower Level</i>	<i>Upper Level</i>	<i>Lower Level</i>	<i>Upper Level</i>
$[(3p_{1/2}^2 3p_{3/2}^3)_{3/2} 3d_{3/2}^2]_{J=3}$	$[(3p_{1/2}^2 3p_{3/2}^2)_0 3d_{3/2}^2 3d_{5/2}^2]_{J=4}$	$[3p_{1/2}^2 3p_{3/2}^3]_{J=3/2}$	$[(3p_{1/2}^2 3p_{3/2}^2)_2 3d_{5/2}^2]_{J=5/2}$
$[3p^6]_{J=0}$	$[3p_{1/2}^2 3p_{3/2}^3 3d_{5/2}^2]_{J=1}$	$[3p_{1/2}^2 3p_{3/2}^3]_{J=3/2}$	$[(3p_{1/2}^2 3p_{3/2}^2)_2 3d_{5/2}^2]_{J=3/2}$
$[(3p_{1/2}^2 3p_{3/2}^3)_{3/2} 3d_{3/2}^2]_{J=3}$	$[(3p_{1/2}^2 3p_{3/2}^2)_2 3d_{3/2}^2]_{7/2} 3d_{5/2}^2]_{J=3}$	$[3p_{1/2}^2 3p_{3/2}^3]_{J=3/2}$	$[(3p_{1/2}^2 3p_{3/2}^2)_0 3d_{5/2}^2]_{J=5/2}$

Table 4. Cont.

W^{58+}		W^{59+}	
<i>Lower Level</i>	<i>Upper Level</i>	<i>Lower Level</i>	<i>Upper Level</i>
$[3p_{1/2}^2 3p_{3/2}^2]_{J=2}$	$[3p_{1/2}^2 3p_{3/2} 3d_{5/2}]_{J=3}$	$[3p_{1/2}^2 3p_{3/2}]_{J=3/2}$	$[3p_{1/2}^2 3d_{5/2}]_{J=5/2}$
$[3p_{1/2}^2 3p_{3/2}^2]_{J=0}$	$[3p_{1/2}^2 3p_{3/2} 3d_{5/2}]_{J=1}$	W^{60+}	
$[3p_{1/2}^2 3p_{3/2}^2]_{J=2}$	$[3p_{1/2}^2 3p_{3/2} 3d_{5/2}]_{J=2}$	<i>Lower Level</i>	<i>Upper Level</i>
$[3p_{1/2}^2 3p_{3/2}^2]_{J=2}$	$[3p_{1/2}^2 3p_{3/2} 3d_{5/2}]_{J=1}$	$[3s_{1/2} 3p_{1/2}^2 3p_{3/2}]_{J=2}$	$[3s_{1/2} 3p_{1/2}^2 3d_{5/2}]_{J=2}$
W^{61+}		$[3p_{1/2} 3p_{3/2}]_{J=2}$	$[3p_{1/2} 3d_{5/2}]_{J=3}$
<i>Lower Level</i>	<i>Upper Level</i>	$[3s_{1/2} 3p_{1/2}^2 3p_{3/2}]_{J=1}$	$[3s_{1/2} 3p_{1/2}^2 3d_{5/2}]_{J=2}$
$[3p_{3/2}]_{J=3/2}$	$[3d_{5/2}]_{J=5/2}$		

4. Present Calculations for M-Shell Excitation of K-like through Ne-like Tungsten Ions

In continuation of our earlier work as described in the previous section on the study of M-shell electron impact excitation of highly charged tungsten ions, we consider here in this paper the $n = 3 \rightarrow 3$ transitions in K-like through Ne-like tungsten ions. Wavelength measurements performed at Super EBIT facility at Livermore for the $n = 3 \rightarrow 3$ transitions in 19–25 Å soft X-ray range for these ions were reported by Clementson *et al.* [19]. In particular, we studied electron impact excitation due to $3s_{1/2} - 3p_{3/2}$ and $3p_{1/2} - 3d_{3/2}$ transitions in potassium like W^{55+} through neon like W^{64+} ions. Magnetic sub-level excitation cross-sections and summed cross-sections as well as polarization of photon after excitation were calculated for the incident electron energies up to 20 keV within the framework of our RDW approach.

We performed tungsten ion structure calculations within multi-configuration Dirac-Fock framework using GRASP2k [33]. A number of CSF's, corresponding to the configurations displayed in Table 5, were included to describe the initial and final states of the tungsten ions. We also calculated the wavefunctions excitation energies and oscillator strengths for all the transitions considered. In Table 6, we compare our values with the available measurements and the theoretical results obtained using FAC and GRASP2 by Clementson *et al.* [19] as well as other calculations [19,48–50,53–55]. Among other calculations are the MCDF calculations of Huang and co-workers [48–51,53] for Cl-like W^{57+} through Al-like W^{61+} ions. In case of Al-3 and Al-4 transitions, Safronova and Safronova [54] used the relativistic many-body perturbation theory (RMBPT) theory. Excitation energies for transitions Cl-3, S-3, P-1 and P-2, are also available from the NIST database [55]. On comparison of excitation energies from the Table 6, we find that our calculations show an overall good agreement with measurements of Clementson *et al.* [19] and their reported FAC calculations [19] for all the ions. It can further be seen from Table 6 that our values for oscillator strengths are within 5% of the only available MCDF calculations for all the transitions except in case of transitions Cl-1 and Cl-3, where the difference between the two theoretical results is, respectively, 14% and 7% [48–51,53]. We hope that the forthcoming measurements as well as other better theoretical calculations will provide more meaningful comparisons.

Utilizing the bound and continuum wavefunctions, we calculated RDW T -matrix (Equation (1)) to get magnetic sublevel cross-sections $\sigma(\alpha_b J_b M_b)$ (Equation (4)) through which the integrated cross-sections could be obtained by summing over all M_b 's. In Figure 1, we display different magnetic sublevel cross-sections $\sigma(\alpha_b J_b M_b)$ along with the total cross-sections for K-like and Ar-like tungsten

ions. This figure shows that for K-1 transition, magnetic excitation cross-section curve for the sublevel $M_b = \pm 3/2$ lies above than that for the corresponding sublevel with $M_b = \pm 1/2$ in the incident electron energy range upto ~ 8 keV and thereafter the behavior is reversed. For K-2 transition where the excitation takes place from the same lower state with $J_a = 3/2$, the cross-sections for the sublevel $M_b = \pm 1/2$ are highest followed by excitation to the sublevels with $M_b = \pm 3/2$ and $M_b = \pm 5/2$ up to an incident electron energy around 8 keV and then the order is reversed. In case of Ar-1, the cross-section for the sublevel with $M_b = 0$ is higher compared to $M_b = \pm 1$ up to an energy of 8 keV and then it becomes less. Thus, we observe a general feature, *i.e.* for each transition, the magnetic sublevels which are more populated in the range of incident energy from the threshold to 8 keV become less populated afterwards. This interesting behavior of the variation of magnetic sublevel cross-sections play an important role in the study of the polarization of the radiation emitted following the decay of the excited states. We will see this later when we discuss Figure 3a for our polarization results corresponding to K-1, K-2 and Ar-1 transitions.

Table 5. CSF's used in GRASP2K [33] code for the representation of target ion wavefunction for the initial and the final states in K-like W^{55+} through Ne-like W^{64+} ions.

<i>K-like</i> W^{55+}	<i>Ar-like</i> W^{56+}	<i>Cl-like</i> W^{57+}	<i>S-like</i> W^{58+}	<i>P-like</i> W^{59+}
		$3s^2 3p^5$		$3s^2 3p^3$
$3s^2 3p^6 3d$		$3s 3p^5 3d$	$3s^2 3p^4$	$3s^2 3p^2 3d$
$3s^2 3p^5 3d^2$	$3s^2 3p^6$	$3p^5 3d^2$	$3s^2 3p^3 3d$	$3s^2 3p 3d^2$
$3s 3p^6 3d^2$	$3s^2 3p^5 3d$	$3s^2 3p^4 3d$	$3s^2 3p^2 3d^2$	$3s 3p^3 3d$
$3p^6 3d^3$	$3s^2 3p^5 4s$	$3s^2 3p^4 4s$	$3s 3p^3 3d^2$	$3s 3p^2 3d^2$
$3s^2 3p^5 4p 4d$	$3s^2 3p^5 4d$	$3s^2 3p^4 4d$	$3s 3p^5$	$3p^5$
$3s 3p^5 3d^3$	$3s^2 3p^5 5s$	$3s 3p^6$	$3p^5 3d$	$3s 3p^4$
		$3p^6 3d$		$3p^4 3d$
<i>Si-like</i> W^{60+}	<i>Al-like</i> W^{61+}	<i>Mg-like</i> W^{62+}	<i>Na-like</i> W^{63+}	<i>Ne-like</i> W^{64+}
				$2s^2 2p^6$
				$2s^2 2p^5 3s$
$3s^2 3p^2$	$3s^2 3p$	$2p^6 3s^2$	$2p^6 3s$	$2s^2 2p^5 3p$
$3s^2 3p 3d$	$3s 3p 3d$	$2p^6 3s 3p$	$2p^6 3p$	$2s^2 2p^5 4p$
$3s^2 3d^2$	$3s^2 3d$	$2p^6 3s 3d$	$2p^5 3p^2$	$2s^2 2p^4 3s 3d$
$3s 3p^3$	$3s 3p^2$	$2p^6 3p^2$	$2p^5 3s 3d$	$2s^2 2p^4 3p^2$
$3s 3p 3d^2$	$3p^2 3d$	$2p^5 3s^2 3p$		$2s^2 2p^4 3d^2$
	$3p^3$			$2s 2p^6 3s$
				$2p^6 3s^2$
				$2p^6 3p^2$

Table 6. Comparison of our calculated excitation energies (in eV) and the oscillator strengths (f) of the transitions in K-like W^{55+} through Ne-like W^{64+} ions with the available measurements and the other theoretical calculations.

<i>Ion</i>	<i>Key</i>	<i>Lower Level</i>	<i>Upper Level</i>	$E_{Present}$	$E_{Measured}[19]$	$E_{FAC}[19]$	$E_{GRASP2} [19]$	$E_{Previous}$	$f_{Present}$	$f_{Previous}$
W^{55+}	K-1	$[3s^2 3p^6 3d_{3/2}]_{J=3/2}$	$[3s^2 (3p_{1/2} 3p_{3/2}^4)_{1/2} 3d_{3/2}^2]_{J=3/2}$	647.19	646.2	647.67	649.88		1.441	
	K-2	$[3s^2 3p^6 3d_{3/2}]_{J=3/2}$	$[3s^2 (3p_{1/2} 3p_{3/2}^4)_{1/2} 3d_{3/2}^2]_{J=5/2}$	601.23	603.27	603.74	602.60		0.385	
W^{56+}	Ar-1	$[3s^2 3p^6]_{J=0}$	$[3s^2 (3p_{1/2} 3p_{3/2}^4)_{1/2} 3d_{3/2}]_{J=1}$	631.80	630.03	631.41	632.35		0.722	
W^{57+}	Cl-1	$[3s^2 3p_{1/2}^2 3p_{3/2}^3]_{J=3/2}$	$[3s^2 (3p_{1/2} 3p_{3/2}^3)_2 3d_{3/2}]_{J=1/2}$	631.01	631.93	633.54	637.71	636.6 ^a	0.217	0.190
	Cl-2	$[3s^2 3p_{1/2}^2 3p_{3/2}^3]_{J=3/2}$	$[3s^2 (3p_{1/2} 3p_{3/2}^3)_2 3d_{3/2}]_{J=3/2}$	624.90	625.74	626.63	628.53	631.7 ^a	0.203	0.196
	Cl-3	$[3s^2 3p_{1/2}^2 3p_{3/2}^3]_{J=3/2}$	$[3s^2 (3p_{1/2} 3p_{3/2}^3)_2 3d_{3/2}]_{J=5/2}$	622.10		624.07	626.53	628.9 ^a 622.9 ^b	0.315	0.294
W^{58+}	S-1	$[3s^2 3p_{1/2}^2 3p_{3/2}^2]_{J=2}$	$[3s^2 (3p_{1/2} (3p_{3/2}^2)_2)_{5/2} 3d_{3/2}]_{J=1}$	628.44	627.7	629.30	632.83	629.76 ^c	0.173	0.177 ^c
	S-2	$[3s^2 3p_{1/2}^2 3p_{3/2}^2]_{J=2}$	$[3s^2 (3p_{1/2} (3p_{3/2}^2)_2)_{5/2} 3d_{3/2}]_{J=2}$	622.54		623.57	627.61	623.92 ^c 622.19 ^b	0.256	0.254 ^c
	S-3	$[3s^2 3p_{1/2}^2 3p_{3/2}^2]_{J=0}$	$[3s^2 (3p_{1/2} (3p_{3/2}^2)_0)_{1/2} 3d_{3/2}]_{J=1}$	623.39		622.35	624.54		0.158	
	S-4	$[3s^2 3p_{1/2}^2 3p_{3/2}^2]_{J=2}$	$[3s^2 (3p_{1/2} (3p_{3/2}^2)_2)_{5/2} 3d_{3/2}]_{J=3}$	615.23	615.40	616.35	619.74	618.29 ^c	0.263	0.262 ^c
	S-5	$[3s^2 3p_{1/2}^2 3p_{3/2}^2]_{J=2}$	$[3s_{1/2} 3p_{1/2}^2 (3p_{3/2}^3)_{3/2}]_{J=2}$	530.35	530.98	531.10	533.33		0.072	

Table 6. Cont.

Ion	Key	Lower Level	Upper Level	$E_{Present}$	$E_{Measured}$ [19]	E_{FAC} [19]	E_{GRASP2} [19]	$E_{Previous}$	$f_{Present}$	$f_{Previous}$
W ⁵⁹⁺	P-1	$[3s^2 3p_{1/2}^2 3p_{3/2}]_{J=3/2}$	$[3s^2 (3p_{1/2} 3p_{3/2})_2 3d_{3/2}]_{J=3/2}$	621.48		622.54	626.53	622.28 ^d 621.20 ^b	0.388	0.364 ^d
	P-2	$[3s^2 3p_{1/2}^2 3p_{3/2}]_{J=3/2}$	$[3s^2 (3p_{1/2} 3p_{3/2})_2 3d_{3/2}]_{J=1/2}$	619.41		621.72	624.73	620.85 ^d 619.00 ^b	0.125	0.129 ^d
	P-3	$[3s^2 3p_{1/2}^2 3p_{3/2}]_{J=3/2}$	$[3s^2 (3p_{1/2} 3p_{3/2})_1 3d_{3/2}]_{J=5/2}$	609.11	610.19	611.21	614.18	610.72 ^d	0.311	0.309 ^d
	P-4	$[3s^2 3p_{1/2}^2 3p_{3/2}]_{J=3/2}$	$[3s_{1/2} 3p_{1/2}^2 (3p_{3/2}^2)_2]_{J=5/2}$	515.43	515.70	515.78	516.67	517.83 ^d	0.042	0.043 ^d
W ⁶⁰⁺	Si-1	$[3s^2 3p_{1/2}^2]_{J=0}$	$[3s^2 3p_{1/2} 3d_{3/2}]_{J=1}$	611.60	611.6	612.90	613.78	611.86 ^e	0.923	0.880 ^e
	Si-2	$[3s^2 3p_{1/2}^2]_{J=0}$	$[3s_{1/2} (3p_{1/2}^2)_0 3p_{3/2}]_{J=1}$	543.63	543.96	544.60	544.65	546.09 ^e	0.172	0.174 ^e
W ⁶¹⁺	Al-1	$[3s^2 3p_{1/2}]_{J=1/2}$	$[3s^2 3d_{3/2}]_{J=3/2}$	597.40	597.34	598.35	600.79	597.88 ^f	0.490	0.476 ^f
	Al-2	$[3s^2 3p_{1/2}]_{J=1/2}$	$[3s_{1/2} (3p_{1/2} 3p_{3/2})_1]_{J=1/2}$	550.99	549.99	550.89	552.76	553.10 ^f	0.212	0.215 ^f
	Al-3	$[3s^2 3p_{1/2}]_{J=1/2}$	$[3s_{1/2} (3p_{1/2} 3p_{3/2})_1]_{J=3/2}$	540.19	539.98	540.24	542.48	542.10 ^f 539.53 ^g	0.116	0.124 ^f 0.103 ^g
	Al-4	$[3s^2 3p_{1/2}]_{J=1/2}$	$[3s_{1/2} (3p_{1/2} 3p_{3/2})_0]_{J=3/2}$	500.60	500.34	500.54	499.65	502.92 ^f 500.34 ^g	0.0020	0.0021 ^f 0.0019 ^g
W ⁶²⁺	Mg-1	$[3s_{1/2} 3p_{1/2}]_{J=1}$	$[3s_{1/2} 3d_{3/2}]_{J=2}$	579.87	580.12	580.45	573.42		0.322	
	Mg-2	$[3s^2]_{J=0}$	$[3s_{1/2} 3p_{3/2}]_{J=1}$	545.03	545.35	546.16	544.87		0.641	
W ⁶³⁺	Na-1	$[3s_{1/2}]_{J=1/2}$	$[3p_{3/2}]_{J=3/2}$	533.27	533.20	533.56	533.28		0.283	
W ⁶⁴⁺	Ne-1	$[2s^2 2p_{1/2}^2 2p_{3/2}^3 3s_{1/2}]_{J=1}$	$[2s^2 2p_{1/2}^2 2p_{3/2}^3 3p_{3/2}]_{J=0}$	588.02	588.51	591.27	591.10		0.052	

^aHuang *et al* [48]; ^b NIST [55]; ^c Chou *et al* [53]; ^d Huang [49]; ^e Huang [50]; ^f Huang [51]; and ^g Safronova and Safronova [54].

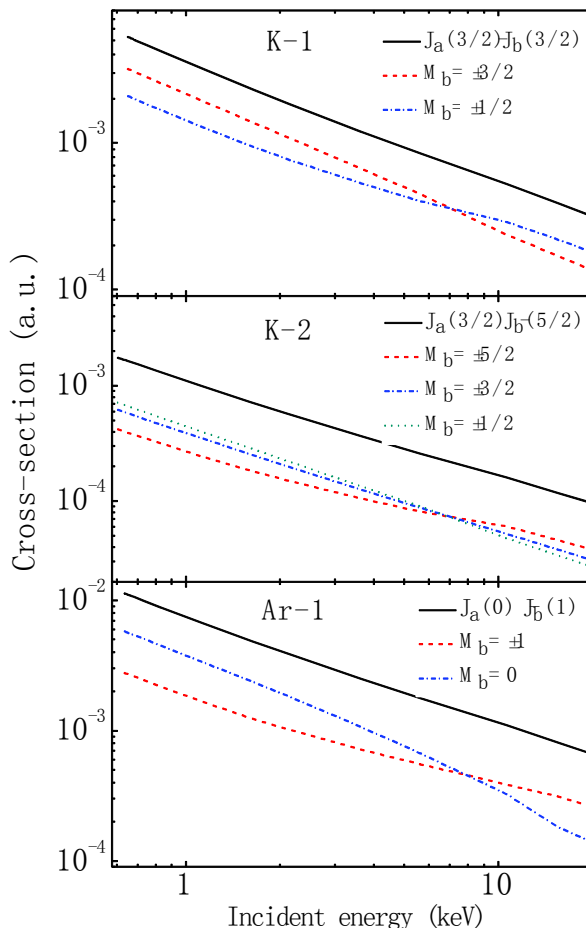


Figure 1. Electron-impact magnetic sublevel and total excitation cross-sections (in atomic units) for K-like and Ar-like tungsten ions as a function of incident electron energy.

Since we are considering many transitions in different tungsten ions with varying values of J_a and J_b , there would be too many corresponding magnetic sublevel cross-section results for each set of J_a and J_b values. Consequently, to avoid crowding of the figures, we only show the total cross-sections for all the transition in Figure 2a,b. These figures show that all the cross-section curves for different transitions decrease linearly right from the threshold to the higher incident electron energies. We also see the general feature that the cross-section for $3s_{1/2} \rightarrow 3p_{3/2}$ transition is always lower than the cross-section for the transition $3p_{1/2} \rightarrow 3d_{3/2}$ for each ion except for Mg-like W^{62+} ion where the reverse is seen.

Analytic fitting of the obtained cross-sections were done using the following formula

$$\sigma = \frac{\sum_{i=0}^n b_i E^i}{c_0 + c_1 E + c_2 E^2} a_0^2 \tag{6}$$

The calculated fitting coefficients are given in the Table 7. These coefficients provide values of cross-sections within an accuracy of 5% right from the excitation threshold impact energy.

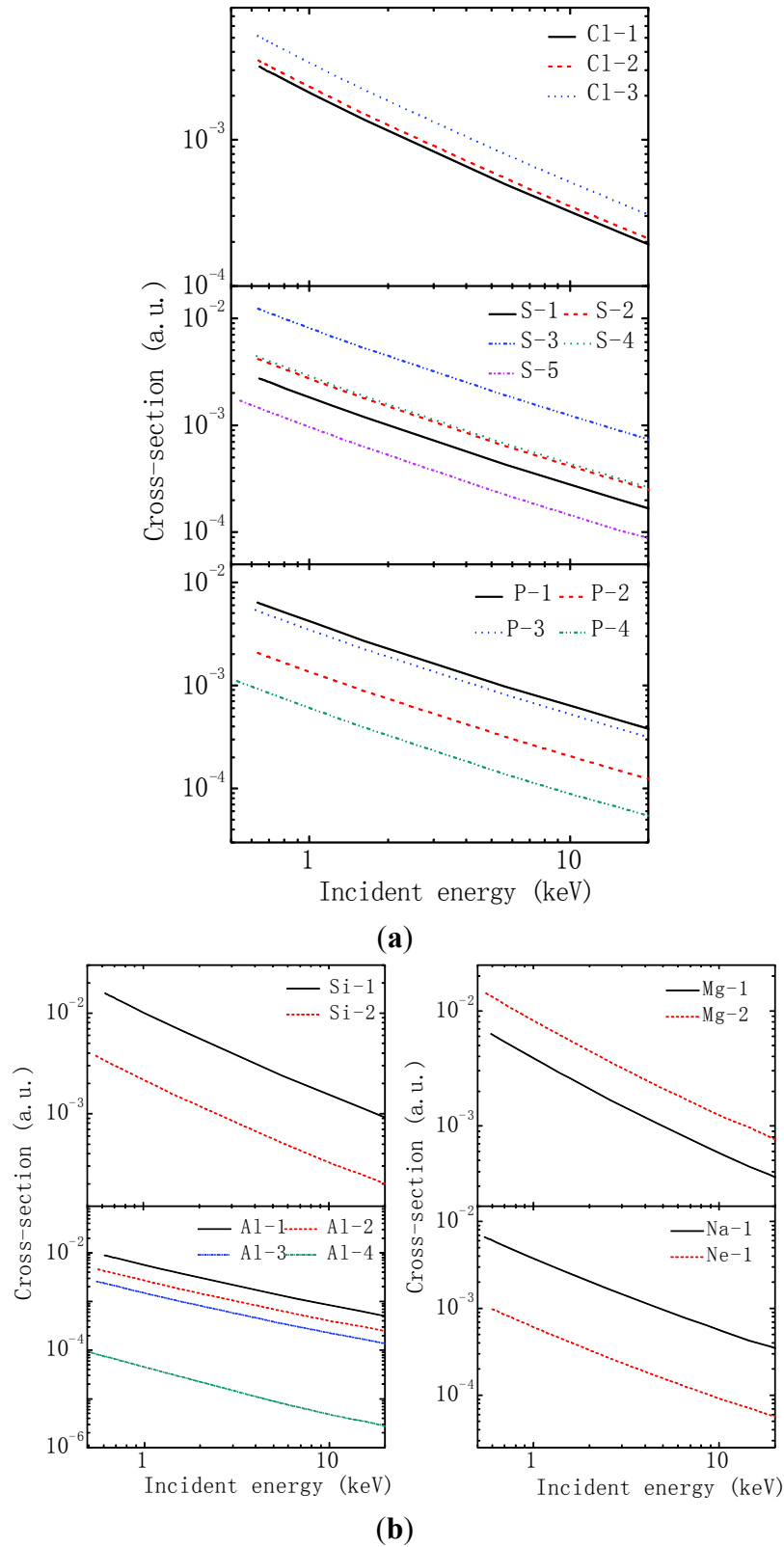
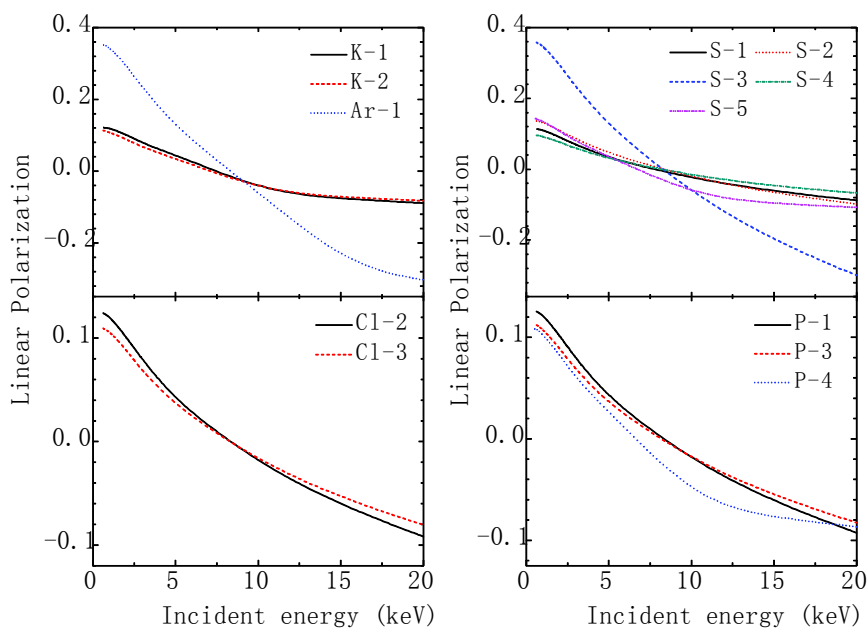


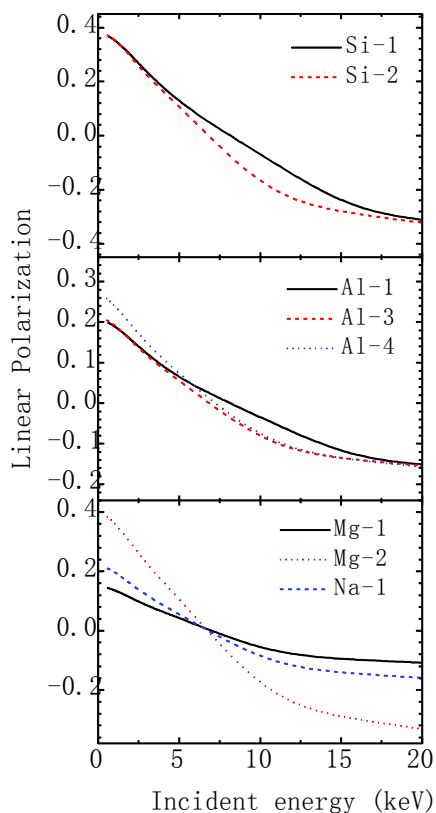
Figure 2. (a) Electron-impact excitation cross-sections (in atomic units) for different transitions as given in Table 6 for Cl-like, S-like and P-like tungsten ions as a function of incident electron energy; (b) Electron-impact excitation cross-sections (in atomic units) for different transitions as given in Table 6 for Si-like, Al-like, Mg-like, Na-like and Ne-like tungsten ions as a function of incident electron energy.

Table 7. Coefficients for the fitting function given in Equation (6) for electron impact excitation cross-sections for all the transitions in K-like W^{55+} through Ne-like W^{64+} ions. The number in the bracket represents the power of 10 by which the quantity has been multiplied.

<i>Ion</i>	<i>Key</i>	b_0	b_1	b_2	b_3	c_0	c_1	c_2
W^{55+}	K-1	3.11677(-1)	2.23638(-3)	8.52164(-7)		5.85249(+1)	2.71204(+0)	9.80664(-3)
	K-2	4.48806(-2)	1.73784(-4)			2.53707(+1)	1.16952(+0)	7.96291(-2)
W^{56+}	Ar-1	1.13969(-2)	4.47742(-4)	5.95543(-10)	3.55779(-5)	7.01913(-1)	1.90273(+0)	7.96291(-2)
W^{57+}	Cl-1	9.25517(-2)	3.81140(-4)			2.88522(+1)	1.27190(+0)	1.90158(-5)
	Cl-2	1.02397(-1)	4.21701(-4)			2.88731(+1)	1.28580(+0)	1.93272(-5)
	Cl-3	1.50742(-1)	6.21858(-4)			2.89651(+1)	1.29560(+0)	1.95184(-5)
W^{58+}	S-1	1.90654(-2)	1.07145(-4)	2.43210(-8)		6.81444(+0)	3.13430(-1)	8.18660(-4)
	S-2	2.88122(-2)	1.61719(-4)	3.63116(-8)		6.81449(+0)	3.16108(-1)	8.23966(-4)
	S-3	8.51184(-2)	4.83359(-4)	1.11054(-7)		6.81631(+0)	3.16292(-1)	8.37729(-4)
	S-4	2.67276(-1)	1.51345(-3)	3.44237(-7)		5.93855(+1)	2.78957(+0)	7.38151(-3)
	S-5	1.02681(-1)	7.06571(-4)	2.65752(-7)		5.93142(+1)	3.29168(+0)	1.18559(-2)
W^{59+}	P-1	8.05453(-2)	3.25370(-4)			1.25106(+1)	5.60198(-1)	8.27364(-4)
	P-2	1.40812(-2)	8.06080(-5)	1.92106(-8)		6.68179(+0)	3.12933(-1)	8.45658(-4)
	P-3	3.64642(-2)	2.10421(-4)	5.02610(-8)		6.68194(+0)	3.18220(-1)	8.69310(-4)
	P-4	3.84554(-3)	3.78456(-5)	3.25047(-8)	1.05095(-11)	3.42358(+0)	2.06440(-1)	1.28072(-3)
W^{60+}	Si-1	4.04866(-1)	1.62130(-3)			2.52737(+1)	1.15084(+0)	1.69347(-3)
	Si-2	9.68220(-2)	3.63716(-4)			2.53397(+1)	1.28431(+0)	1.65007(-3)
W^{61+}	Al-1	9.04079(-3)	2.48386(-7)	1.16146(-3)		3.36091(-3)	3.04110(+0)	1.34588(-1)
	Al-2	4.64005(-3)	1.12413(-7)	6.48106(-4)		2.40066(-3)	3.04169(+0)	1.45958(-1)
	Al-3	2.63551(-3)	1.23729(-4)	9.72385(-11)	1.30408(-5)	3.73498(-1)	2.13835(+0)	1.05531(-1)
	Al-4	9.14755(-5)	4.86592(-6)	3.16316(-12)	3.54016(-7)	1.35241(+0)	1.37690(+0)	7.26933(-2)
W^{62+}	Mg-1	1.61410(-1)	5.05668(-4)			2.53830(+1)	1.16343(+0)	1.22164(-3)
	Mg-2	3.76691(-1)	1.39624(-3)			2.60676(+1)	1.31803(+0)	1.67008(-3)
W^{63+}	Na-1	2.05206(-2)	7.74583(-5)			3.02309(+0)	1.56720(-1)	2.10181(-4)
W^{64+}	Ne-1	3.02868(-3)	1.05254(-5)			3.02448(+0)	1.41603(-1)	1.66132(-4)



(a)



(b)

Figure 3. (a) Polarization for the photon emission from anisotropic excited states through different transitions (as given in Table 6) for K-like, Ar-like, Cl-like, S-like and P-like tungsten ions as a function of incident electron energy; (b) Polarization for the photon emission from anisotropic excited states through different transitions (as given in Table 6) for Si-like, Al-like, Mg-like and Na-like tungsten ions as a function of incident electron energy.

Magnetic sub-level excitation cross-sections are further utilized to calculate the polarization of emitted photons following the decay of electron impact excited states using the formulae given in Table 1. Results obtained for polarization due to the decay from the final state with J_b to a lower level with J_0 are shown in the Figure 3a,b. According to the density matrix theory it is clearly evident that if the polarization of incoming electrons is not accounted for, $\sigma(\alpha_b J_b M_b)$ will be equal for the two magnetic substates with the same mod value of M_b *i.e.*, $\sigma(M_b) = \sigma(-M_b)$. Thus, the excited state with $J_b = 1/2$ is not aligned; consequently, the degree of linear polarization of the photon emission would be zero. Hence, the polarization for the transitions *viz.* Cl-1, P-2, Al-2 decaying from the excited states with $J_b = 1/2$ are not displayed in these figures. Another transition Ne-1 following the decay from $J_b = 0$ to $J_0 = 1$ give an isotropic photon emission, and its polarization is also zero. The two Figures 3a and b illustrate a general expected behavior *i.e.*, polarization decreases with the increase of incident electron energy for all the transitions considered. For most of the transitions, polarization attains negative values around 8 keV. The two types of decay transitions considered *viz.* $3p_{3/2} \rightarrow 3s_{1/2}$ and $3d_{3/2} \rightarrow 3p_{1/2}$, exhibit different shapes of polarization curves for all the ions. We find that for the decay from $J_b = 1$ to $J_0 = 0$ in transitions *viz.*, Ar-1, Si-1, Si-2, S-3 and Mg-2, the polarization near threshold is quite large and nearly 40%.

5. Conclusions

We presented a brief overview of our recent work on the study of electron impact L- and M-shell excitations of highly charged Ne-like through Co-like tungsten ions using a fully relativistic distorted wave theory. This work was undertaken in the light of EBIT measurements on L- and M-shell spectra of these ions. New calculations are performed to obtain cross-sections and polarization of the emitted photon for various transitions in K-like through Ne-like tungsten ions and results are reported in the present paper in the wide range of incident electron energies up to 20 keV. Fitting of the new cross-section results is also provided to fulfill the purpose of serving atomic data for fusion plasma diagnostics.

Acknowledgments

Rajesh Srivastava and Lalita Sharma would like to acknowledge research grants for this work from the Department of Atomic Energy, Govt. of India (DAE-BRNS). Rajesh Srivastava is also grateful to the International Atomic Energy Agency (IAEA), Vienna, Austria for a grant in partial support of this research. Dipti and Priti are thankful to the Council of Scientific and Industrial Research (CSIR), New Delhi and the Ministry of Human Resource Development, Government of India (MHRD), respectively, for providing financial assistance.

Author Contributions

Priti and Dipti proposed the main idea of the paper and carried out all the calculations. They also wrote some parts of manuscript. Lalita Sharma and Rajesh Srivastava provided the computer code and hardware. They were also involved in the discussions of results and in writing the manuscript.

Conflicts of Interest

The authors declare no conflict of interest.

References

1. Neu, R.; Dux, R.; Kallenbach, A.; Pütterich, T.; Balden, M.; Fuchs, J.C.; Herrmann, A.; Maggi, C.F.; O'Mullane, M.; Pugno, R.; *et al.* Tungsten: An option for divertor and main chamber plasma facing components in future fusion devices. *Nucl. Fusion* **2005**, *45*, 209–218.
2. Ikeda, K. ITER on the road to fusion energy. *Nucl. Fusion* **2010**, *50*, 014002:1–014002:10.
3. Merolaa, M.; Loesserb, D.; Martina, A.; Chappuisa, P.; Mitteaua, R.; Komarova, V.; Pitts, R.A.; Gicquela, S.; Barabasha, V.; Giancarlia, L.; *et al.* ITER plasma-facing components. *Fusion Eng. Des.* **2010**, *85*, 2312–2322.
4. Inubushi, Y.; Kai, T.; Nakamura, T.; Fujioka, S.; Nishimura, H.; Mima, K. Analysis of x-ray polarization to determine the three-dimensionally anisotropic velocity distributions of hot electrons in plasma produced by ultrahigh intensity lasers. *Phys. Rev. E* **2007**, *75*, 026401:1–026401:5.
5. Beiersdorfer, P.; Slater, M. Measurement of the electron cyclotron energy component of the electron beam of an electron beam ion trap. *Phys. Rev. E* **2001**, *64*, 066408:1–066408:6.
6. Skinner, C.H. Atomic physics in the quest for fusion energy and ITER. *Phys. Scr.* **2009**, *134*, 014022:1–014022:4.
7. CRP on spectroscopic and collisional data for tungsten. Available online: <https://www-amdis.iaea.org/CRP/Tungsten/> (accessed on 21 January 2015).
8. Watanabe, H.; Nakamura, N.; Kato, D.; Nakano, T.; Ohtani, S. X-Ray Spectra from Neon-like Tungsten Ions in the Interaction with Electrons. *Plasma Fusion Res. Rapid Commun.* **2007**, *2*, 27:1–27:3.
9. Ralchenko, Y.; Draganić, I.N.; Tan, J.N.; Gillaspay, J.D.; Pomeroy, J.M.; Reader, J.; Feldman, U.; Holland, G.E. EUV spectra of highly-charged ions W^{54+} – W^{63+} relevant to ITER diagnostics. *J. Phys. B* **2008**, *41*, 021003:1–021003:6.
10. Peacock, N.J.; O' Mullane, M.G.; Barnsley, R.; Tarbutt, M. Anticipated X-ray and VUV spectroscopic data from ITER with appropriate diagnostic instrumentation. *Can. J. Phys.* **2008**, *86*, 277–284.
11. Pütterich, T.; Neu, R.; Dux, R.; Whiteford, A.D.; O'Mullane, M.G. The ASDEX Upgrade Team Modelling of measured tungsten spectra from ASDEX Upgrade and predictions for ITER. *Plasma Phys. Control. Fusion* **2008**, *50*, 085016:1–085016:26.
12. Biedermann, C.; Radtke, R.; Seidel, R.; Pütterich, T. Spectroscopy of highly charged tungsten ions relevant to fusion plasmas. *Phys. Scr.* **2009**, *134*, 014026:1–014026:6.
13. Clementson, J.; Beiersdorfer, P.; Brown, G.V.; Gu, M.F.; Lundberg, H.; Podpaly, Y.; Träbert, E. Tungsten spectroscopy at the Livermore electron beam ion trap facility. *Can. J. Phys.* **2011**, *89*, 571–580.
14. Ralchenko, Y.; Draganić, I.N.; Osin, D.; Gillaspay, J.D.; Reader, J. Spectroscopy of diagnostically important magnetic-dipole lines in highly charged $3d^n$ ions of tungsten. *Phys. Rev. A* **2011**, *83*, 032517:1–032517:10.
15. Kramida, A. Recent progress in spectroscopy of tungsten. *Can. J. Phys.* **2011**, *89*, 551–575.
16. Beiersdorfer, P.; Brown, G.V.; Graf A.T.; Bitter, M.; Hill K.W.; Kelley R.L.; Kilbourne C.A.; Leutenegger, M.A. Porter F.S. Rest-wavelength fiducials for the ITER core imaging x-ray spectrometer. *Rev. Sci. Instrum.* **2012**, *83*, 10E111:1–10E111:3.

17. Gillaspay, J.D.; Osin, D.; Ralchenko, Y.; Reader, J.; Blundell, S.A. Transition energies of the D lines in Na-like ions. *Phys. Rev. A* **2013**, *87*, 062503:1–062503:10.
18. Clementson, J.; Beiersdorfer, P.; Brown, G.V.; Gu, M.F. Spectroscopy of M-shell x-ray transitions in Zn-like through Co-like W. *Phys. Scr.* **2010**, *81*, 015301:1–015301:8.
19. Clementson, J.; Beiersdorfer, P. Wavelength measurement of $n = 3$ to $n = 3$ transitions in highly charged tungsten ions. *Phys. Rev. A* **2010**, *81*, 052509:1–052509:7.
20. Clementson, J.; Beiersdorfer, P.; Gu, M.F. X-ray spectroscopy of E2 and M3 transitions in Ni-like W. *Phys. Rev. A* **2010**, *81*, 012505:1–012505:6.
21. Beiersdorfer, P.; Lepson, J.K.; Schneider, M.B.; Bode, M.P. L-shell x-ray emission from neonlike W^{64+} . *Phys. Rev. A* **2012**, *86*, 012509:1–012509:10.
22. Lennartsson, T.; Clementson, J.; Beiersdorfer, P. Experimental wavelengths for intrashell transitions in tungsten ions with partially filled 3p and 3d subshells. *Phys. Rev. A* **2013**, *87*, 062505:1–062505:7.
23. Beiersdorfer, P.; Clementson, J.; Dunn, J.; Gu, M.F.; Morris, K.; Podpaly, Y.; Wang, E.; Bitter, M.; Feder, R.; Hill, K.W.; *et al.* The ITER core imaging x-ray spectrometer. *J. Phys. B* **2010**, *43*, 144008:1–144008:10.
24. Fujimoto, T.; Iwamae, A., Eds.; *Plasma Polarization Spectroscopy*; Springer Berlin Heidelberg: New York, NY, USA, 2008; Volume 44.
25. Das, T.; Sharma, L.; Srivastava, R. Electron impact excitation of the M-shell electrons from Zn-like through Co-like tungsten ions. *Phys. Scr.* **2012**, *86*, 035301:1–035301:11.
26. Dipti; Das, T.; Sharma, L.; Srivastava, R. L-shell electron excitations of Mg- through O-like tungsten ions. *Phys. Scr.* **2014**, *89*, 085403:1–085403:13.
27. Dipti; Das, T.; Sharma, L.; Srivastava, R. Electron impact excitation and polarization studies of Fe-like W^{48+} to Al-like W^{61+} ions. *Can. J. Phys.* **2015**, in press.
28. Gangwar, R.K.; Sharma, L.; Srivastava, R.; Stauffer, A.D. Argon plasma modeling with detailed fine-structure cross sections. *J. Appl. Phys.* **2012**, *111*, 053307:1–053307:9.
29. Sharma, L.; Surzhykov, A.; Srivastava, R.; Fritzsche, S. Electron-impact excitation of singly charged metal ions. *Phys. Rev. A* **2011**, *83*, 062701:1–062701:8.
30. Madison, D.H.; Bartschat, K. *The Distorted-Wave Method for Elastic Scattering and Atomic Excitation, Computational Atomic Physics: Electron and Positron Collision with Atoms and Ions*; Bartschat, K., Ed.; Springer-Verlag: Berlin/Heidelberg, Germany, 1996.
31. Srivastava, R.; Stauffer, A.D.; Sharma, L. Excitation of the metastable states of the noble gases. *Phys. Rev. A* **2006**, *74*, 012715:1–012715:10.
32. Parpia, F.A.; Fischer, C.F.; Grant, I.P. GRASP92: A package for large-scale relativistic atomic structure calculations. *Comput. Phys. Commun.* **1996**, *94*, 249–271.
33. Jönsson, P.; He, X.; Fischer, C.F.; Grant, I.P. The grasp2K relativistic atomic structure package. *Comput. Phys. Commun.* **2007**, *177*, 597–622.
34. Balashov, V.V.; Grum-Grzhimailo, A.N.; Kabachnik, N.M. *Polarization and Correlation Phenomena in Atomic Collisions*; Kluwer Academic/Plenum: New York, NY, USA, 2000.
35. Chen, M.H.; Crasemann, B. Systematic trends of the oscillator strengths for $n = 3$ and 2 electric dipole transitions in oxygen-like ions. *Phys. Rev. A* **1989**, *40*, 4330:1–4330:7.
36. Ivanova, E.P.; Gulov, A.V. Theoretical investigation of the neon isoelectronic sequence. *At. Data Nucl. Data Tables* **1991**, *49*, 1–64.

37. Vilkas, M.J.; López-Encarnación, J.M.; Ishikawa, Y. Relativistic multireference Møller–Plesset perturbation theory calculations of the energy levels and transition probabilities in Ne-like xenon, tungsten, and uranium ions. *At. Data Nucl. Data Tables* **2008**, *94*, 50–70.
38. Safronova, U.I.; Safronova, A.S.; Beiersdorfer, P. Excitation energies, radiative and autoionization rates, dielectronic satellite lines, and dielectronic recombination rates for excited states of Na-like W from Ne-like W. *At. Data Nucl. Data Tables* **2009**, *95*, 751–785.
39. Safronova, U.I.; Safronova, A.S.; Beiersdorfer, P. Excitation energies, radiative and autoionization rates, dielectronic satellite lines and dielectronic recombination rates for excited states of Mg-like W from Na-like W. *J. Phys. B* **2009**, *42*, 165010:1–165010:17.
40. Zhang, H.L.; Sampson, D.H. Relativistic distorted wave collision strengths for excitation to the $n = 3$ and $n = 4$ levels in all 71 neon-like ions with $22 \leq Z \leq 92$. *At. Data Nucl. Data Tables* **1989**, *43*, 1–69.
41. Sampson, D.H.; Zhang, H.L.; Fontes, C.J. Relativistic distorted wave collision strengths and oscillator strengths for the 71 Na-like ions with $22 \leq Z \leq 92$. *At. Data Nucl. Data Tables* **1990**, *44*, 209–271.
42. Sampson, D.H.; Zhang, H.L.; Fontes, C.J. Relativistic distorted-wave collision strengths and oscillator strengths for F-like ions with $22 \leq Z \leq 92$. *At. Data Nucl. Data Tables* **1991**, *48*, 25–90.
43. Zhang, H.L.; Sampson, D.H. Relativistic Distorted-wave collision strengths and oscillator strengths for the $45 \Delta n = 0$ transition with $n = 2$ in the 79 O-like ions with $14 \leq Z \leq 92$. *At. Data Nucl. Data Tables* **2002**, *82*, 357–389.
44. Zhang, H.L.; Sampson, D.H.; Fontes, C.J. Relativistic distorted wave collision strengths and oscillator strengths for the 33 Cu-like ions with $60 \leq Z \leq 92$. *At. Data Nucl. Data Tables* **1990**, *44*, 273–304.
45. Zhang, H.L.; Sampson, D.H.; Fontes, C.J. Relativistic distorted-wave collision strengths and oscillator strengths for the 33 Ni-like ions with $60 \leq Z \leq 92$. *At. Data Nucl. Data Tables* **1991**, *48*, 91–163.
46. Xie, L.Y.; Ma, X.Y.; Dong, C.Z.; Wu, Z.W.; Shi, Y.L.; Jiang, J. Polarization of the $nf \rightarrow 3d$ ($n = 4, 5, 6$) x-rays from tungsten ions following electron-impact excitation and dielectronic recombination processes. *J. Quant. Spectrosc. Radiat. Transf.* **2014**, *141*, 31–39.
47. Fournier, K.B. Atomic data and spectral line intensities for highly ionized tungsten (Co-like W^{47+} to Rb-like W^{37+}) in a high-temperature, low density plasma. *At. Data Nucl. Data* **1998**, *68*, 1–48.
48. Huang, K.N.; Kim, Y.K.; Cheng, K.T. Energy-level scheme and transition probabilities of Cl-like ions. *At. Data Nucl. Data Tables* **1983**, *28*, 355–377.
49. Huang, K.H. Energy-level scheme and transition probabilities of P-like ions. *At. Data Nucl. Data Tables* **1984**, *30*, 313–421.
50. Huang, K.H. Energy-level scheme and transition probabilities of Si-like ions. *At. Data Nucl. Data Tables* **1985**, *32*, 503–566.
51. Huang, K.N. Energy-level scheme and transition probabilities of Al-like ions. *At. Data Nucl. Data Tables* **1986**, *34*, 1–77.
52. Seely, J.F.; Brown, C.M.; Behring, W.E. Transitions in Fe-, Co-, Cu-, and Zn-like ions of W and Re. *J. Opt. Soc. Am. B* **1989**, *6*, 3–6.
53. Chou, H.S.; Chang, J.Y.; Chang, Y.S.; Huang, K.N. Energy-level scheme and transition probabilities of S-like. *At. Data Nucl. Data Tables* **1996**, *62*, 77–145.

54. Safronova, U.I.; Safronova, A.S. Wavelengths and transition rates for $n'l-n'l'$ transitions in Be-, B-, Mg-, Al-, Ca-, Zn-, Ag- and Yb-like tungsten ions. *J. Phys. B* **2010**, *43*, 074026:1–074026:15.
55. Kramida, A.; Ralchenko, Y.; Reader, J.; NIST ASD Team. NIST Atomic Spectra Database (ver. 5.2). Available Online: <http://physics.nist.gov/asd> (accessed on 11 November 2014).

© 2015 by the authors; licensee MDPI, Basel, Switzerland. This article is an open access article distributed under the terms and conditions of the Creative Commons Attribution license (<http://creativecommons.org/licenses/by/4.0/>).